

The low-extinction afterglow in the solar-metallicity host galaxy of γ -ray burst 110918A \star

J. Elliott¹, T. Krühler², J. Greiner¹, S. Savaglio¹, F. Olivares E.¹, A. Rau¹, A. de Ugarte Postigo^{3,2}, R. Sánchez-Ramírez³, K. Wiersema⁴, P. Schady¹, D. A. Kann^{5,1}, R. Filgas^{6,1}, M. Nardini⁷, E. Berger⁸, D. Fox⁹, J. Gorosabel^{3,11,12}, S. Klose⁵, A. Levan¹⁰, A. Nicuesa Guelbenzu⁵, A. Rossi⁵, S. Schmid⁵, V. Sudilovsky¹, N. R. Tanvir⁴, and C. C. Thöne³

¹ Max-Planck-Institut für extraterrestrische Physik, Giessenbachstraße 1, 85748, Garching, Germany.
e-mail: jonnyelliott@mpe.mpg.de

² Dark Cosmology Centre, Niels Bohr Institute, University of Copenhagen, Juliane Maries Vej 30, 2100, Copenhagen, Denmark.

³ Instituto de Astrofísica de Andalucía (IAA-CSIC), Glorieta de la Astronomía s/n, E-18008, Granada, Spain.

⁴ The University of Leicester, Department of Physics and Astronomy, University Road, Leicester, LE1 7RH, United Kingdom.

⁵ Thüringer Landessternwarte Tautenburg, Sternwarte 5, 07778, Tautenburg, Germany.

⁶ Institute of Experimental and Applied Physics, Czech Technical University in Prague, Horská 3a/22, 12800, Prague, Czech Republic.

⁷ Università degli studi di Milano-Bicocca, Piazza della Scienza 3, 20126, Milano, Italy.

⁸ Harvard-Smithsonian Center for Astrophysics, 60 Garden Street, Cambridge, MA 02138, USA.

⁹ Department of Astronomy & Astrophysics, 525 Davey Laboratory, Pennsylvania State University, University Park, PA 16802, USA.

¹⁰ Department of Physics, University of Warwick, Coventry CV4 7AL, UK.

¹¹ Unidad Asociada Grupo Ciencia Planetarias UPV/EHU-IAA/CSIC, Departamento de Física Aplicada I, E.T.S. Ingeniería, Universidad del País Vasco UPV/EHU, Alameda de Urquijo s/n, E-48013 Bilbao, Spain.

¹² Ikerbasque, Basque Foundation for Science, Alameda de Urquijo 36-5, E-48008 Bilbao, Spain.

Received 20 December 2012 / Accepted 30 May 2013

ABSTRACT

Galaxies selected through long γ -ray bursts (GRBs) could be of fundamental importance when mapping the star formation history out to the highest redshifts. Before using them as efficient tools in the early Universe, however, the environmental factors that govern the formation of GRBs need to be understood. Metallicity is theoretically thought to be a fundamental driver in GRB explosions and energetics, but is still, even after more than a decade of extensive studies, not fully understood. This is largely related to two phenomena: a dust-extinction bias, that prevented high-mass and thus likely high-metallicity GRB hosts to be detected in the first place, and a lack of efficient instrumentation, that limited spectroscopic studies including metallicity measurements to the low-redshift end of the GRB host population. The subject of this work is the very energetic GRB 110918A ($E_{\gamma, \text{iso}} = 1.9 \times 10^{54}$ erg), for which we measure a redshift of $z = 0.984$. GRB 110918A gave rise to a luminous afterglow with an intrinsic spectral slope of $\beta = 0.70$, which probed a sight-line with little extinction ($A_V^{\text{GRB}} = 0.16$ mag) and soft X-ray absorption ($N_{\text{H,X}} = (1.6 \pm 0.5) \times 10^{21} \text{ cm}^{-2}$) typical of the established distributions of afterglow properties. Photometric and spectroscopic follow-up observations of the galaxy hosting GRB 110918A, including optical/NIR photometry with GROND and spectroscopy with VLT/X-shooter, however, reveal an all but average GRB host in comparison to the $z \sim 1$ galaxies selected through similar afterglows to date. It has a large spatial extent with a half-light radius of $R_{1/2} \sim 10$ kpc, the highest stellar mass for $z < 1.9$ ($\log(M_*/M_\odot) = 10.68 \pm 0.16$), and an $H\alpha$ -based star formation rate of $\text{SFR}_{H\alpha} = 41^{+28}_{-16} M_\odot \text{ yr}^{-1}$. We measure a gas-phase extinction of $A_V^{\text{gas}} \sim 1.8$ mag through the Balmer decrement and one of the largest host-integrated metallicities ever of around solar using the well-constrained ratios of $[\text{N II}]/H\alpha$, and $[\text{N II}]/[\text{O II}]$ ($12 + \log(\text{O}/\text{H}) = 8.93 \pm 0.13$ and $8.85^{+0.14}_{-0.18}$, respectively). This presents one of the very few robust metallicity measurements of GRB hosts at $z \sim 1$, and establishes that GRB hosts at $z \sim 1$ can also be very metal rich. It conclusively rules out a metallicity cut-off in GRB host galaxies and argues against an anti-correlation between metallicity and energy release in GRBs.

Key words. Gamma-ray burst: general, Gamma-ray burst: individual: GRB 110918A, ISM: general, Galaxies: abundances, Galaxies: photometry, Galaxies: star formation

1. Introduction

During their prompt emission, long gamma-ray bursts (GRBs) are the brightest objects in the Universe, easily reaching isotropic-equivalent luminosities as high as $\sim 10^{54} \text{ erg s}^{-1}$. Their

observed association to supernovae events (e.g., Galama et al. 1998; Hjorth et al. 2003; Stanek et al. 2003; Matheson et al. 2003; Della Valle 2011; Hjorth et al. 2012) has tightly linked them to the death of massive stars. The GRB itself is then believed to result from accretion of matter onto the newly formed rapidly rotating black hole or compact object in the collapsar model (Woosley 1993; Paczynski 1998; MacFadyen & Woosley 1999). The lack of hydrogen and helium in the spectra of GRB-

\star Based on observations made with telescopes at the European Southern Observatory at La Silla/Paranal, Chile under program 090.A-0760(A).

supernovae classify them as type Ic, supporting the notion that GRB progenitors are likely Wolf-Rayet like stars (for a review of supernova classifications see, e.g., Filippenko 1997). Given that these type of stars undergo vigorous mass loss from stellar winds, metallicity constraints ($Z < 0.3 Z_{\odot}$) on the progenitor are postulated to ensure that an accretion disk is still formed around the black hole (Hirschi et al. 2005; Yoon & Langer 2005; Woosley & Heger 2006).

The possible association of long GRBs with massive stars supported the idea that they could be used as complementary and independent tracers of star formation, especially at high redshifts ($z \geq 4$), due to their very high luminosities (see e.g., Daigne et al. 2006; Li 2008; Kistler et al. 2009; Ishida et al. 2011). However, to have full confidence in these studies the intrinsic evolutionary effects in long GRB production must be understood and the galactic environments preferred by the progenitor need to be quantified (e.g., Butler et al. 2010; Wang & Dai 2011; Salvaterra et al. 2012; Robertson & Ellis 2012; Elliott et al. 2012). Of particular interest is the relation between the galaxies selected by GRBs and the star formation weighted population of field galaxies. To be direct and unbiased tracers of star formation, the relative rates of GRBs in galaxies of various physical properties should be the same in galaxies taken from samples that trace the global star formation density at a given redshift. Studies based on these galaxy samples are most commonly performed at $z \lesssim 1.5$, where the star formation of field galaxies is largely recovered by state-of-the-art deep-field surveys.

Initial work showed that many long GRB host galaxies had a low mass, low metallicity, as well as blue colours and were actively star forming (see e.g., Fruchter et al. 1999; Le Floch et al. 2003; Berger et al. 2003; Christensen et al. 2004; Tanvir et al. 2004). This seemed directly in line with the requirements of the collapsar model. Further work carried out with larger samples (e.g. Savaglio et al. 2009), showed again similar characteristics. However, at a given mass and star formation rate, long GRB hosts were also found to be no different to the normal population of star forming galaxies at the same redshift (Mannucci et al. 2011). However, these initial studies neglected the contribution from galaxies hosting dust-extinguished afterglows, often termed dark bursts (e.g., Perley et al. 2009; Greiner et al. 2011). Galaxies hosting dark bursts are systematically more massive and have a higher dust-content than the previously-established population localized with optically bright afterglows (Krühler et al. 2011; Hjorth et al. 2012; Rossi et al. 2012; Perley et al. 2013; Christensen et al. 2011; de Ugarte Postigo et al. 2012). Despite the inclusion of this more evolved galaxy population, there are still less GRBs in massive galaxies than expected based on their contribution to the overall star formation rate (SFR), at least at $z < 1.5$ (Perley et al. 2013), indicative of a GRB explosion mechanism dependent on metallicity. It is however important to note that these above conclusions are inferred indirectly through stellar mass as a metallicity proxy, and while the photometric samples of GRB hosts have reached integrated number statistics of 100 and above (e.g., Hjorth et al. 2012; Perley et al. 2013), the most crucial measurement of gas-phase metallicity has only been performed in a hand-full cases at $z \gtrsim 1$ (Levesque et al. 2010a; Krühler et al. 2012a).

Only a few host galaxies with substantial gas-phase metallicities around or above solar (e.g., Levesque et al. 2010b) that directly violate the proposed cut-off in galaxy metallicity have been observed to date. There is thus still lively debate in the literature about the nature of GRB hosts, and their relation to the star formation weighted galaxy population as a whole (e.g., Niino 2011; Mannucci et al. 2011; Kocevski & West 2011; Graham

& Fruchter 2012). GRB hosts with high stellar mass and high global metallicity are hence of primary interest for GRB host studies, as they directly probe this allegedly forbidden parameter space. A robust understanding of the galactic environments in which GRBs form would then add confidence in their use as cosmological probes, beyond the limits of deep survey studies (e.g., Tanvir et al. 2012; Basa et al. 2012).

Here, we present spectroscopy and photometry of the host galaxy and afterglow of the luminous GRB 110918A, detected on the 18th of September 2011 at $T_0=21:26:57$ UT (Hurley et al. 2011). This burst had one of the highest fluences of any GRB observed over the last 20 years (together with GRB 021206; Wigger et al. 2008) and had the highest peak flux ever detected by *Konus-Wind* (Golenetskii et al. 2011; Frederiks & Pal'shin 2011, Frederiks et al. 2013 in prep.), located at a redshift of $z = 0.98$. The massive, metal rich host galaxy and unobscured afterglow of GRB 110918A challenges the current view of the connection between local and global environments and allow us to investigate the preferred conditions for the formation of a long GRB.

The paper is arranged as follows: first we describe the observations carried out by both ground and space based instruments and their corresponding reduction in Sect. 2. Second, the resulting properties ascertained from the SEDs and spectra of the GRB and its host are described in Sect. 3. Finally, we discuss our findings and their implications for the population of long GRBs in Sect. 4 and conclude in Sect. 5. We adopt the convention that the GRB flux density is described by $F_{\nu}(t) \propto t^{-\alpha} \nu^{-\beta}$, reported errors are at the 1σ confidence level and we assume a Λ CDM cosmology: $H_0 = 71 \text{ km s}^{-1} \text{ Mpc}^{-1}$, $\Omega_M = 0.27$ and $\Omega_{\Lambda} = 0.73$. We use a Chabrier (2003) initial mass function and abundances throughout the text.

2. Observations and Data Reduction

2.1. *Swift* -XRT Spectra

At the time of the IPN trigger *Swift* (Gehrels et al. 2004) was both in the South Atlantic Anomaly and Earth-occulted, and so no trigger (Krimm & Siegel 2011) was initiated in the Burst Alert Telescope (Barthelmy et al. 2005, BAT). However, the *Swift* X-ray telescope (Burrows et al. 2005, XRT) began observing the field of GRB 110918A (see Fig. 1) at $T_0 + 107.4$ ks until ~ 40 d later. The XRT spectrum shows no signs of spectral evolution, remaining with a constant hardness ratio of ~ 0.85 for its entire emission. We extract a spectrum at the time interval of $T_0 + 140$ ks to $T_0 + 250$ ks to coincide with our optical/NIR wavelength observations (see Fig. 2). The XRT spectral data were obtained from the public *Swift* archive and were regrouped to ensure at least 20 counts per bin in the standard manner, using the *grappa* task from the HEASoft package with response matrices from CALDB v20120209. We assume a Galactic hydrogen column of $N_{\text{H,X}}^{\text{Gal}} = 1.68 \times 10^{20} \text{ cm}^{-2}$ (Kalberla et al. 2005) in the direction of the burst.

2.2. GROND Optical/NIR Photometry

The Gamma-Ray Burst Optical Near-infrared Detector (GROND; Greiner et al. 2008) mounted at the MPG/ESO 2.2 m telescope at La Silla, Chile, began its follow-up campaign of GRB 110918A 29.2 hrs after the trigger simultaneously in the $g'r'i'z'JHK_s$ filters (Elliott et al. 2011). A mosaic of 5 pointings was carried out to cover the full IPN error box ($\sim 20' \times 20'$) and the GRB optical afterglow candidate

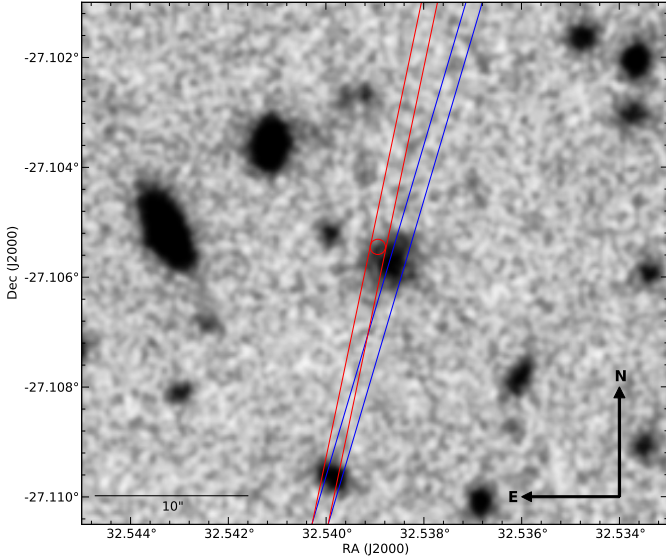


Fig. 1: A GROND 60 minute stacked i' band image of the GRB 110918A host galaxy. The slit arrangement used in the acquisition image is shown for both the OSIRIS afterglow spectrum (red line) and host spectrum (blue line).

was detected at the location R.A. (J2000) = $02^h10^m09.34^s$, Dec. (J2000) = $-27^\circ06'19.7''$, in GROND’s NIR chips, located just outside the IPN error box, consistent with the X-ray (Mangano et al. 2011) and optical (Tanvir et al. 2011) position with an uncertainty of $0.2''$. GROND observations continued for over 1 month after the GRB trigger and an underlying host was discovered (see also Oksanen et al. 2011). Deep images of 3600 s in the NIR and 4500 s in the optical were obtained with GROND of the host galaxy at $T_0 + 36.37$ d.

Image reduction and photometry of the GROND observations were carried out using standard IRAF tasks (Tody 1993) in the way outlined in Krühler et al. (2008) and Yoldaş et al. (2008). In brief, a point-spread function (PSF) was obtained from the bright stars within the field and applied to the afterglow photometry. The absolute calibration of the optical photometry was achieved by observing a Sloan Digital Sky Survey (SDSS) field (Aihara et al. 2011) at R.A. (J2000) = $01^h40^m00.0^s$, Dec. (J2000) = $-18^\circ03'00.0''$ and the GRB field consecutively. The NIR absolute calibration was obtained from the Two Micron Sky Survey (2MASS) stars (Skrutskie et al. 2006) within the field of the GRB. As a result of the extension of the galaxy (see Fig. 1) an aperture size of $3.2''$ was used on the deep host galaxy images, within which the aperture flux flattened in a curve-of-growth analysis and the zero points were correspondingly corrected.

The scope of this paper does not involve a full analysis of the afterglow emission. However, afterglow flux measurements are required at certain time intervals to implement slit loss corrections to the optical spectra and to determine the local extinction of the afterglow. Therefore, we only present the required data and direct the reader to future work for a full analysis of the afterglow¹. For the slit loss correction of the afterglow, we obtain the following brightnesses in the AB system at a mid time of $T_0 + 2.2$ d: $g' = 20.50 \pm 0.05$ mag, $r' = 20.20 \pm 0.04$ mag, $i' = 19.96 \pm 0.04$ mag, $z' = 19.83 \pm 0.07$ mag, $J = 19.46 \pm 0.09$ mag, $H = 19.04 \pm 0.10$ mag, $K_s = 18.66 \pm 0.19$ mag. The magnitudes

¹ For the interested reader the afterglow light curves are found in the Appendix.

are uncorrected for a Galactic dust reddening of $E(B - V)^{Gal} = 0.020$ mag corresponding to an extinction of $A_V^{Gal} = 0.062$ mag for $R_V = 3.1$ (Schlegel et al. 1998).

2.3. WFI Optical Photometry

Further deep observations of the host galaxy were made 392 d after the trigger with the Wide Field Imager (Baade et al. 1999, WFI), also mounted on the MPG/ESO 2.2m telescope, in the standard broadband filters BB#B/123_ESO878 (B) and BB#U/150_ESO878 (U). Two sets of images were taken, the first on 25 October 2012 consisting of 1800 s in U and 600 s in B and the second set was on 26 October 2012, consisting of 150 s in U and 75 s in B . A calibration field was obtained on 26 October 2012 in both the U and B filters and the standard field SA113+158² was used as a primary calibrator. The photometry was carried out in the same way as the GROND images, and the magnitudes converted into the AB system using the ESO magnitude converter³.

2.4. WISE IR Photometry

The Wide-field Infrared Survey Explorer (Wright et al. 2010, WISE) All-Sky Source Catalogue⁴ reveals a source at the position of the host galaxy of GRB 110918A, with an 11σ and 3σ detection in the $W1$ and $W2$ bands, centred at $3.4\mu\text{m}$ and $4.6\mu\text{m}$ respectively. The *wmpro* magnitudes were used, which are the magnitudes retrieved from profile-fitting photometry (or the magnitude of the 95% confidence brightness) and converted into the AB system using the WISE conversion factors⁵. Galactic reddening corrections were made using the A_V^{Gal} conversions determined by Jarrett et al. (2012).

2.5. GMOS Optical Spectroscopy

The first spectrum of the afterglow was taken with the Gemini Multi-Object Spectrographs (Hook et al. 2004, GMOS) on the Gemini North telescope (Mauna Kea) starting at 12:52 UT on 20 September 2011, 1.6 d after the GRB trigger. Four exposures of 500 s each were obtained using the R400 grism and a $1''$ (~ 8.0 kpc projected at $z = 0.984$) slit width. Two of the spectra were obtained with a central wavelength of 6000 \AA and the other two with 6050 \AA to cover the detector gaps. In addition, a spatial dither was used to cover the amplifier boundaries. The resulting spectrum covers the range $3930 - 8170 \text{ \AA}$. We reduced the data with tasks within the *Gemini.GMOS* package and *IRAF*, v1.11, using flat field and arc lamp frames taken directly before and after the science data.

2.6. OSIRIS Optical Spectroscopy

The second spectrum of the afterglow was obtained using the Optical System for Imaging and low Resolution Integrated Spectroscopy (Cepa et al. 2000, OSIRIS) mounted on the 10.4 m Gran Telescopio Canarias (Roque de los Muchachos) starting at 13:00 UT on 21 September 2011, 2.2 d after the GRB trig-

² www.eso.org/sci/observing/tools/standards/Landolt.html

³ <http://archive.eso.org/mag2flux>

⁴ <http://irsa.ipac.caltech.edu>

⁵ http://wise2.ipac.caltech.edu/docs/release/allsky/expsup/sec4_4h.html

ger. Three exposures of 900 seconds each were taken using the R500B grism and a $1''$ slit width obtained at the parallactic angle. The resulting spectrum covers the range 4400–8700 Å. Data were reduced and calibrated using standard procedures in IRAF. The spectrum was flux calibrated using G157-34 as a standard star and the 1D spectrum was scaled to the GROND afterglow photometry to correct for slit losses (correction factor of ~ 1.9).

A spectrum of the host was obtained on 11 November 2011, $T_0 + 54.1$ d after the GRB trigger. A sequence of three 1200 s exposures were obtained with OSIRIS using the R1000R grism and a $1.0''$ slit width, covering the wavelength range of 5100 Å to 10000 Å. The spectrum was flux calibrated using the standard star G191-B2B and corrected for slit losses by scaling the 1D spectrum to the photometry of the host galaxy obtained using GROND (correction factor of ~ 3.5).

2.7. X-Shooter Optical/NIR Spectroscopy

We further observed the host of GRB 110918A with the cross-dispersed echelle spectrograph X-shooter (Vernet et al. 2011) on the Very Large Telescope Kueyen (UT2). X-shooter has three individual arms taking spectra simultaneously in the range of 3000 Å to 5600 Å (UVB arm), 5600 Å to 10200 Å (VIS arm), and 10200 Å to 24800 Å (NIR arm). Three different sets of observations were carried out on 17 December 2012, 07 January 2013, and 16 January 2013, respectively, with a position angle of 59° East of North. They consisted of a pair of nodded frames with exposure times of 1200 s in each of the UVB/VIS arm and 2×600 s in the NIR arm. The slit width was $1''.6$, $1''.5$ and $0''.9$ yielding a resolution measured on arc-lamp frames of $R \sim \lambda/\Delta\lambda = 3200$, 4900, and 5300 in the UVB, VIS and NIR arm, respectively. The NIR slit includes a blocking filter for the *K*-band limiting our effective wavelength coverage to < 20500 Å, but providing lower background levels in the *J* and *H*-band.

Each of the individual observations were reduced and wavelength- and flux-calibrated separately using standard procedures within the X-shooter pipeline `v2.0.0` (Goldoni et al. 2006) supplied by ESO. The individual two-dimensional frames were then stacked using variance weighting in a heliocentric reference frame, and the one-dimensional spectra were extracted using an optimal extraction method. Given the extent of the target, slit-losses are substantial. Similar to the OSIRIS and GMOS spectroscopy, we scaled the well-detected continuum of the X-shooter data to the available photometric host SED. The consistency between matching factors derived from different photometric data in the individual arms⁶, provides confidence that the absolute flux-calibration in the final X-shooter spectrum is accurate to better than $\sim 20\%$ over the full wavelength range of interest.

3. Results

3.1. The Afterglow Sight-Line: Dust, Star Formation Rate and Gas

A broadband SED was constructed from the optical/NIR GROND photometry (see Sect. 2.2) at a mid time of $T_0 + 194$ ks and X-ray data between $T_0 + 140$ ks and $T_0 + 250$ ks. The SED

⁶ We derive factors for the r' -, i' - and z' -band data in the VIS arm of 3.1 ± 0.3 , 2.8 ± 0.3 , 2.8 ± 0.3 , and 3.5 ± 0.4 , 3.3 ± 0.3 for the *J* and *H*-band in the NIR arm. The offset between the VIS and NIR arm is readily explained by the smaller slit width in the NIR arm.

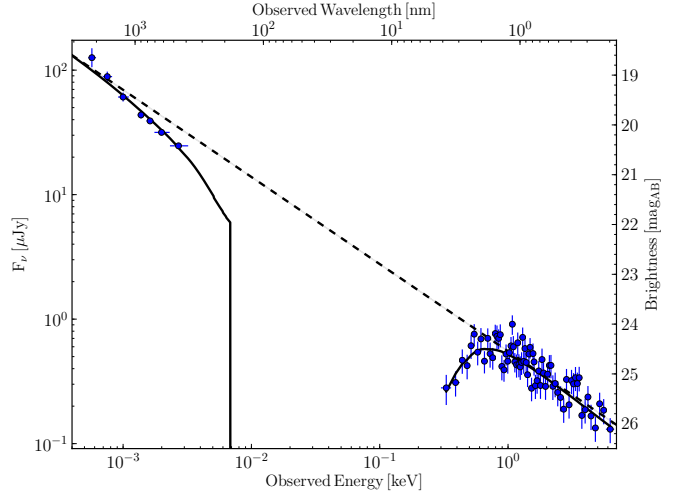


Fig. 2: Broadband SED of GRB 110918A, including optical, NIR and X-ray data. The SED was constructed using GROND data at a mid time of $T_0 + 194$ ks and X-ray data between $T_0 + 140$ ks and $T_0 + 250$ ks. The best-fit parameters for a power-law ($\chi^2/\text{d.o.f.} = 85/73$) are: a spectral slope of $\beta = 0.70 \pm 0.02$, a hydrogen column density of $N_{\text{H,X}}^{\text{GRB}} = 1.56^{+0.52}_{-0.46} \times 10^{21} \text{ cm}^{-2}$ and a line of sight extinction of $A_V^{\text{GRB}} = 0.16 \pm 0.06 \text{ mag}$, assuming SMC like dust.

was fit in a standard manner (e.g., Filgas et al. 2011), assuming that the afterglow emission is well described by the standard synchrotron mechanism. The best fit single power-law ($\chi^2/\text{d.o.f.} = 85/73$) is shown in Fig. 2 with a spectral slope of $\beta = 0.70 \pm 0.02$, a hydrogen column density of $N_{\text{H,X}}^{\text{GRB}} = 1.56^{+0.52}_{-0.46} \times 10^{21} \text{ cm}^{-2}$ and a line of sight extinction of $A_V^{\text{GRB}} = 0.16 \pm 0.06 \text{ mag}$, assuming a Small Magellanic Cloud (SMC) like dust with $R_V = 2.93$ in the parametrization of Pei (1992). Despite yielding an improved fit, a broken power-law model is not warranted as the number of free parameters increases ($\chi^2/\text{d.o.f.} = 83/71$), implying the improvement is not statistically significant. Nevertheless, the resulting parameters of the best fit broken power-law, as well as from different dust models, are consistent with the uncertainties of the power-law values below the break at ~ 0.6 keV and do not alter our conclusions.

Using the procedure outlined by de Ugarte Postigo et al. (2012) with the two afterglow spectra obtained with GMOS ($T_0 + 1.6$ d) and OSIRIS ($T_0 + 2.2$ d), we detect the transition of several metal ions including Fe II, Mg II and Mg I at a common redshift of $z = 0.984 \pm 0.001$ (see Tables 2 and B.1), consistent with galactic winds or star bursting periods (Fynbo et al. 2009; Nestor et al. 2011; Christensen et al. 2011; Rodríguez Hidalgo et al. 2012). In comparison with a long GRB sample (de Ugarte Postigo et al. 2012) we find that it has stronger absorption features than 80% of the sample.

3.2. The Host's Stellar Component: Dust Attenuation, Star Formation Rate and Stellar Mass

The host of GRB 110918A was detected in 11 different filters ranging from the ultra-violet to $4.5\mu\text{m}$, yielding a well-sampled photometric SED (see Fig. 3 and Table 1). To estimate the global properties of the host galaxy we employed standard techniques that use stellar population synthesis to estimate stellar masses, as outlined thoroughly in Ilbert et al. (2009). We con-

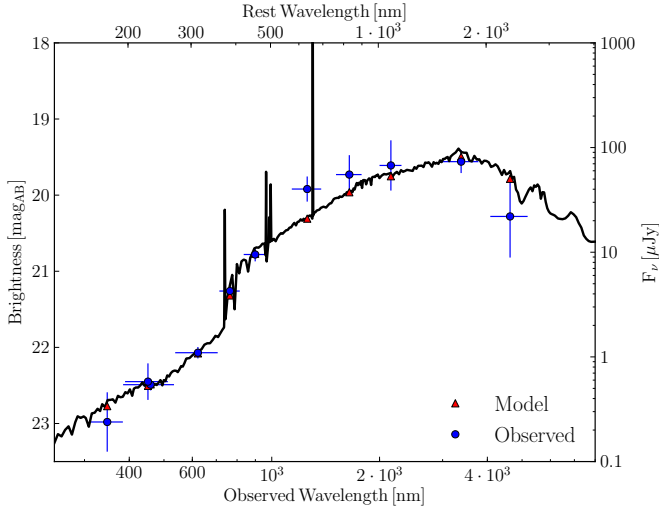


Fig. 3: The SED of the host of GRB 110918A obtained using GROND, WFI and WISE data, amounting to 11 filters: $UBg'r'i'z'JHK_sW1W2$ from left to right. The best-fit spectrum is depicted in black.

structured a grid of galaxy templates based on the models taken from Bruzual & Charlot (2003) over a wide parameter space consisting of: a range of ages ($0 - 1.35 \times 10^9$ yr), star formation histories ($\propto e^\tau$, $\tau = 0.1, 0.3, 1, 2, 3, 5, 10, 15, 30$), reddening values ($E(B - V) = 0 - 0.4$ mag), a single attenuation law (starburst; Calzetti et al. 2000) and metallicities ($Z = 0.004, 0.008, 0.02$). Emission lines were also included, whereby the emission lines were estimated from the predicted UV luminosity and converted to a star formation rate using Kennicutt (1998). For each template a SED was constructed for the filters required and a χ^2 was calculated using the Photometric Analysis for Redshift Estimate routines, LePHARE ⁷ v2.2 (Arnouts et al. 1999; Ilbert et al. 2006). The best fit template was the one that gave the minimum χ^2 and the corresponding uncertainties for each parameter were obtained from the grid of χ^2 values. Systematic uncertainties of up to an average of 0.2 – 0.3 dex are expected in the stellar mass value due to the adopted stellar population models and extinction laws (see e.g., Krühler et al. 2011, and references therein). The filter response curves for the W1 and W2 bands were obtained from Wright et al. (2010) and for the U and B bands from the ESO web pages⁸. The results of the best fit template, which had a $\chi^2/\# \text{Bands} = 5.4/11$, had the following parameters: a mass of $\log_{10} \left(\frac{M_*}{M_\odot} \right) = 10.68 \pm 0.16$, a star formation rate $\text{SFR}_{\text{SED}} = 66_{-30}^{+50} M_\odot$, a reddening of $E(B - V)^{\text{stars}} = 0.26 \pm 0.15$ mag, and a starburst age of $\tau = 0.7_{-0.4}^{+1.4}$ Gyr.

3.3. The Host's Gas-Phase Component: Dust Extinction, Star Formation Rate and Metallicity

The first host spectrum of GRB 110918A was obtained with OSIRIS/GTC in the optical wavelength range, ~ 50 days after the trigger, and the one second was obtained with X-shooter/VLT more than 460 days post trigger. The X-shooter spectrum extends our spectral coverage to the NIR and thus to

Table 1: Host galaxy magnitudes.

Filter	Instrument	Magnitude (mag _{AB})	Uncertainty (mag _{AB})
U	WFI	22.98	0.25
B	WFI	22.45	0.16
g'	GROND	22.49	0.15
r'	GROND	22.07	0.05
i'	GROND	21.26	0.06
z	GROND	20.78	0.06
J	GROND	19.92	0.11
H	GROND	19.73	0.17
K _s	GROND	19.61	0.22
W1	WISE	19.56	0.10
W2	WISE	20.28	0.36

Notes. Corrected for Galactic foreground reddening. The observations in $g'r'i'z'JHK_s$ were obtained 36.37 d after the burst. The UB observations were obtained 392 d after the burst. The W1 and W2 photometry were obtained prior to the burst by the WISE Survey.

the wavelength range where important tracers of star formation rate and metallicity are located. In summary, we clearly detect the $H\alpha$ and $H\beta$ transition from the Balmer series, as well as the forbidden transitions of $[\text{O II}](\lambda\lambda 3726, 3729)$ and $[\text{N II}](\lambda 6584)$. The emission lines corresponding to $[\text{O III}](\lambda\lambda 4959, 5007)$ are cosmologically redshifted to regions of low sensitivity for both OSIRIS and X-shooter, and are thus not detected.

The velocity profile of the emission lines is clearly resolved by our X-shooter data and spans approximately 500 km s^{-1} in velocity space (see Fig. C.1). It displays a conspicuous two-humped profile, with the two peaks of the emission lines separated by 200 km s^{-1} . However, we do not observe a spatial tilt in the line-shape as would have been expected from a largely rotationally-supported galaxy (unless it is face on), and both peaks appear at the same spatial position in the two-dimensional spectrum. Line fluxes were measured by numerically integrating the available data, and cross-checked with fitting Gaussians. Both procedures return consistent values, and from the X-shooter spectrum, we measure global⁹ emission-lines fluxes of $f_{[\text{O II}]} = (19.0 \pm 3.1) \times 10^{-17} \text{ erg s}^{-1} \text{ cm}^{-2}$, $f_{H\beta} = (9.5 \pm 1.9) \times 10^{-17} \text{ erg s}^{-1} \text{ cm}^{-2}$, $f_{H\alpha} = (47.8 \pm 4.9) \times 10^{-17} \text{ erg s}^{-1} \text{ cm}^{-2}$ and $f_{[\text{N II}]} = (15.3 \pm 3.3) \times 10^{-17} \text{ erg s}^{-1} \text{ cm}^{-2}$. The OSIRIS spectrum yields $f_{[\text{O III}]} = (20.0 \pm 2.8) \times 10^{-17} \text{ erg s}^{-1} \text{ cm}^{-2}$, fully consistent with the X-shooter value.

Assuming case B recombination (Osterbrock 1989) and using the standard values for electron density ($10^2 \text{ cm}^{-3} \lesssim n_e \lesssim 10^4 \text{ cm}^{-3}$) and temperature ($T_e \sim 10^4 \text{ K}$), the Balmer ratio of $H\alpha/H\beta$ implies an $E(B - V)^{\text{gas}} = 0.57_{-0.22}^{+0.24}$ or visual extinction $A_V^{\text{gas}} = 1.8_{-0.7}^{+0.8}$ mag towards the star forming regions assuming a Milky-Way like extinction law¹⁰. It is worth mentioning, that this is the luminosity-weighted reddening/extinction of the gas-phase. This value is typically found to be a factor of around two larger than the stellar $E(B - V)^{\text{stars}}$ from the photometric SED model (e.g., Calzetti et al. 2000), consistent with our measurements for GRB 110918A. The $H\alpha$ line flux implies a SFR

⁹ Here and in the following, the error includes both the statistical error of the measurement as well as the error in slit-loss correction.

¹⁰ Different local extinction laws yield comparable results, as there is little difference in the wavelength range of the $H\alpha$ and $H\beta$ Balmer lines.

⁷ www.cfht.hawaii.edu/~arnouts/LEPHARE/lephare.html

⁸ www.eso.org/sci/facilities/lasilla/instruments/wfi/inst/filters

Table 2: Physical parameters of the galaxy hosting GRB 110918A

Quantity	Unit/Method	Value
$E(B - V)^{\text{GRB}}$	mag	0.05 ± 0.02
$N_{\text{X,H}}^{\text{GRB}}$	10^{21} cm^{-2}	$1.56^{+0.52}_{-0.46}$
$\text{EW}_{\text{rest}}^{\text{GRB}}$	(Å) Mg II(2796, 2803)	6.0
$\text{SFR}_{\text{[OII]}}^{\text{GRB}}$	$M_{\odot} \text{ yr}^{-1}$	2.3 ± 0.7
Stellar Mass	$\log(M_*/M_{\odot})$	10.69 ± 0.16
Half-light radius	kpc	10
$E(B - V)^{\text{stars}}$	mag	0.26 ± 0.15
SFR_{SED}	$M_{\odot} \text{ yr}^{-1}$	66^{+50}_{-30}
τ	Gyr	$0.7^{+1.4}_{-0.4}$
$\text{SFR}_{\text{H}\alpha}$	$M_{\odot} \text{ yr}^{-1}$	41^{+28}_{-16}
$E(B - V)^{\text{gas}}$	mag	$0.57^{+0.24}_{-0.22}$
$12 + \log(\text{O}/\text{H})$	[N II]/H $\alpha^{(a)}$	8.93 ± 0.13
$12 + \log(\text{O}/\text{H})$	[N II]/H $\alpha^{(b)}$	8.63 ± 0.08
$12 + \log(\text{O}/\text{H})$	[N II]/[O II] ^(a)	$8.86^{+0.10}_{-0.14}$
$12 + \log(\text{O}/\text{H})$	[N II]/[O II] ^(c)	$8.85^{+0.14}_{-0.18}$

Notes. All values use a Chabrier IMF, and take into account the statistical uncertainty of the measurements, as well as the uncertainty in the slit-loss and dust-correction factor if applicable. ^(a) Following Nagao et al. (2006). ^(b) Following Pettini & Pagel (2004). ^(c) Following Kewley & Dopita (2002).

of $\text{SFR}_{\text{H}\alpha} = 41^{+28}_{-16} M_{\odot} \text{ yr}^{-1}$, following Kennicutt (1998) with a Chabrier (2003) IMF.

Using the different emission line ratios, we can measure the gas-phase metallicity of the galaxy hosting GRB 110918A (see e.g., Kewley & Ellison 2008, for an extensive summary on those techniques). At $z \sim 1$ we are limited to the diagnostic ratios based on H α , [O II] and [N II]. When using the ratio of [N II] and H α as a metallicity tracer, uncertainties in the reddening or chromatic slit-losses are not going to affect the overall results, because the respective lines are located very close in wavelength space. However, [N II]/H α saturates at high metallicities ([N II]/H $\alpha \sim 0.3$), while [N II]/[O II] does not. The final uncertainties are thus comparable in both indicators, and we measure $12 + \log(\text{O}/\text{H})_{\text{N2H}\alpha} = 8.93 \pm 0.13$ and $12 + \log(\text{O}/\text{H})_{\text{N2O2}} = 8.85^{+0.14}_{-0.18}$ using the formulation of Nagao et al. (2006). Different calibrations of the strong-line diagnostics yield $12 + \log(\text{O}/\text{H})_{\text{N2H}\alpha} = 8.63 \pm 0.08$ (Pettini & Pagel 2004) or $12 + \log(\text{O}/\text{H})_{\text{N2O2}} = 8.86^{+0.10}_{-0.14}$ (Kewley & Dopita 2002). The inherent systematic uncertainty of typically 0.1-0.2 dex (e.g., Nagao et al. 2006; Kewley & Ellison 2008) has not been included. These measurements imply metallicities between 0.9 and 1.7 times solar. All physical parameters of the galaxy hosting GRB 110918A are summarized in Table 2.

4. Discussion

4.1. Host Galaxy Identification

We have used absorption lines from metal ions in the afterglow spectrum (see also Fynbo et al. 2009, for an extensive sample), and forbidden/recombination lines from the host galaxy to determine the redshift of the GRB (see also Krühler et al. 2012b), but it is in principle possible that the GRB lies at a higher redshift. To investigate if the host galaxy of GRB 110918A has been misidentified we calculate the commonly used p-value, $p(m) = 1 - \exp(-\pi r_i^2 \sigma(\leq m))$, which is the probability of finding a galaxy of magnitude m (or brighter) overlapping the GRB

within an effective radius r_i , assuming that galaxies are Poisson distributed throughout the sky (Bloom et al. 2002). This neglects any type of galaxy clustering, however, recent work indicates that GRB locations do not preferentially lie in areas of strong galaxy overabundances (Cucchiara et al. 2012; Sudilovsky et al. 2013). The number of galaxies brighter than m per square arcsecond is given by σ , taken from Bloom et al. (2002) and calculated from the work of Hogg et al. (1997).

The burst location of GRB 110918A is seen to be offset from the bright centroid of the host by 12 kpc, however, in comparison to the half-light radius of the host galaxy, $R_{1/2} = 10.6$ kpc, the offset is consistent with the long GRB population, which has a median offset of $R_{\text{offset}}/R_{1/2} \sim 1$ (Bloom et al. 2002). We follow Bloom et al. (2002) and set $r_i = 2 \times R_{1/2} = 2.66''$. Synthetic R_C -band (Bessell 1979) photometry of the GRB 110918A host galaxy using the best fit galaxy template taken from Sect. 3.2, and the conversions given in Rossi et al. (2012), results in $R_C = 21.7 \text{ mag}_{\text{Vega}}$. This yields a probability of chance association of $p = 0.01$, making this galaxy highly likely the host of GRB 110918A.

The non-detection of the Lyman forest above $\sim 4500 \text{ \AA}$ implies a strong upper limit of $z < 2.7$. Therefore, using our knowledge of the strength of spectral features in GRB environments and their distribution (de Ugarte Postigo et al. 2012), we can estimate the likelihood of the GRB having occurred between redshift 1.0 and 2.7 and yet not having detectable absorption lines at the redshift of the host in its spectrum. We calculate the detection limits for Mg II and C IV doublets as described by de Ugarte Postigo et al. (2012) and find that the lines would have to be weaker than 99.7% of a normal long GRB sample to have happened at a redshift between 1 and 2.7. Furthermore, the properties of the absorber (strong Mg II absorption and vigorous star formation, see Sect. 3.1), are very common in other afterglow observations, and do not indicate a different physical nature. Combining the arguments presented above, we consider the redshift of the GRB, and accordingly the physical association between GRB and galaxy, robust.

4.2. Host Environment in the Context of the GRB-Host Population

The mass-metallicity relation of field galaxies (e.g., Tremonti et al. 2004) has been studied in depth to high redshift (Savaglio et al. 2005; Erb et al. 2006; Yabe et al. 2012). Similarly, the dust content of a given galaxy is also well known to correlate with stellar mass (e.g., Garn & Best 2010; Zahid et al. 2013). To illustrate the behaviour for GRB hosts, we show the average host galaxy extinction versus the stellar mass of the host galaxy alongside the correlation determined by Garn & Best (2010) in Fig. 4. The GRB hosts are taken from Savaglio et al. (2009, SG09), Mannucci et al. (2011, MN11), Krühler et al. (2011, KR11) and Perley et al. (2013, PL13) and converted to a Chabrier IMF if need be. The correlation of Garn & Best (2010) has been determined from SDSS galaxies with $z < 0.7$ and so we limited our GRB sample to galaxies with $z < 1.0$. GRB hosts follow the distribution obtained from field galaxies well, with a possible excess of dusty systems at stellar masses of $10^9\text{-}10 M_{\odot}$. Given the inherent systematic difficulties of determining the dust reddening in galaxies, and the heterogeneous selection of targets (in particular the KR11 and PL13 samples were initially selected to contain a lot of dust), this trend should not be over-interpreted. What seems clear is that the host of GRB 110918A is at the high end of the distribution of stellar masses for GRB hosts, and

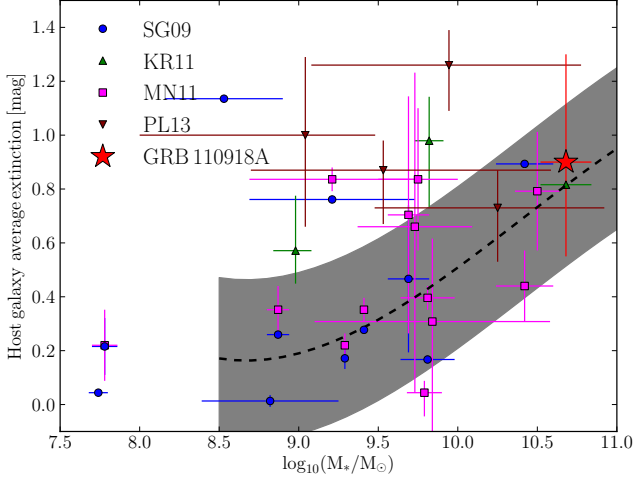


Fig. 4: The average line of sight extinction of the host galaxy vs. the stellar mass. Values from SG09 and MN11 have been converted from $E(B - V)^{\text{gas}}$ to $E(B - V)^{\text{stars}}$ using the relation from Calzetti et al. (2000). The dotted-black line is the polynomial fit determined by Garn & Best (2010) and the grey region denotes the uncertainty of 0.3 dex.

there is no strong discrepancy between GRB-selected galaxies and field galaxies in the relation between their dust content and stellar mass.

Secondly we plot the host’s stellar mass vs. the GRB’s line of sight extinction in Fig. 5. Perley et al. (2013) have highlighted that throughout the covered galaxy-mass scale, there is a very tight correlation between stellar-mass and sight-line extinction probed by the GRBs. Quite surprisingly, this correlation between afterglow dust and galaxy mass is found to be stronger than for any other physical property of the galaxy (PL13). From Fig. 5 it can be seen that hosts selected due to high afterglow extinction (green, KR11; brown PL13) have systematically more massive and dust extinguished sight lines than the optically selected hosts (blue, SG09). Outliers to this trend such as GRB 061222A or GRB 100621A have already been noted (e.g., Krühler et al. 2011; Perley et al. 2009), that were within blue, low-mass galaxies that were locally strongly extinguished along the line of sight. GRB 110918A is the first example of a dust-poor line of sight with a galaxy mass at the high-end of the distribution (i.e., $\log_{10}\left(\frac{M_*}{M_{\odot}}\right) > 10.5$). While in principle, cases like GRB 110918A would be easy to identify (bright afterglow, easy localization, bright host), no comparable example has been reported in the literature to date.

The host of GRB 110918A shows similar host-integrated extinction ($A_V^{\text{stars}} = 0.90$ mag) to galaxies of a similar mass range (e.g., $M_* > 10^{10} M_{\odot}$ in Fig. 4 and $M_* > 4 \times 10^9 M_{\odot}$ in Fig. 15 of Perley et al. (2013) have an $A_V^{\text{stars}} \gtrsim 1.0$ mag). However, in comparison to the systems of similar mass, GRB 110918A exhibits at least 10 times less extinction along the GRB line of sight. Therefore, it is possible that: (i) the geometry of dust within the host of GRB110918A is more patchy than homogeneous in comparison to the rest of the massive GRB host population, in agreement with the example of GRB 100621A and 061222A, whereby clumpy dust was one explanation for having a highly extinguished afterglow within an unobscured galaxy (Krühler et al. 2011; Perley et al. 2013), or (ii) the pro-

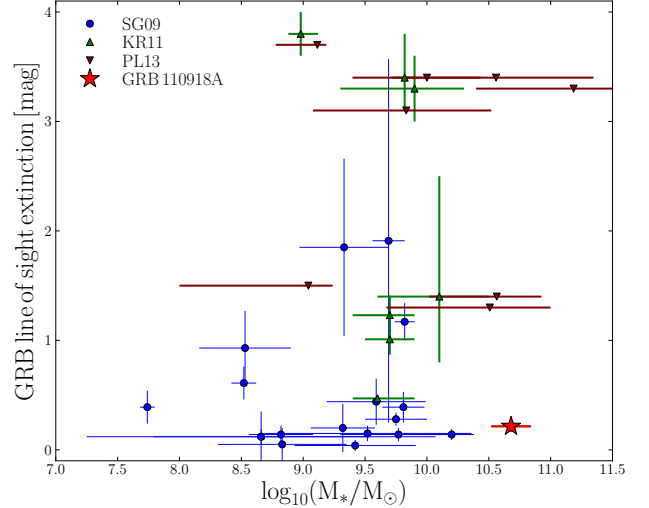


Fig. 5: The GRB line of sight A_V^{GRB} plotted against the stellar mass of the host galaxy. The extinction values have been obtained from Kann et al. (2006), Kann et al. (2010), Greiner et al. (2011), Schady et al. (2012) and Perley et al. (2013).

genitor had enough time to destroy local dust from its UV emission (see Perley et al. 2013, and references therein).

4.3. Fundamental Metallicity Relation

The difference between galaxies of long GRBs and that of normal star forming field galaxies is still an on going debate. We have derived estimates for the mass, metallicity and SFR of the host of GRB 110918A, which facilitates comparing this galaxy with respect to normal star forming galaxies through the fundamental metallicity relation (FMR; Mannucci et al. 2011). The plane of the FMR was derived from star forming SDSS galaxies in the mass range $9.2 < \log_{10}\left(\frac{M_*}{M_{\odot}}\right) < 11.4$ and is described by:

$$12 + \log(O/H) = 8.90 + 0.47 \times (\mu_{0.32} - 10), \quad (1)$$

where $\mu_{0.32} = \log_{10}(M_*/M_{\odot}) - 0.32 \times \log(\text{SFR}/M_{\odot}\text{yr}^{-1})$. Using the SED-determined mass and the $H\alpha$ -determined SFR, the metallicity from the FMR is $12 + \log(O/H) = 8.98 \pm 0.08$, in agreement with the metallicity from the $\text{N II}/H\alpha$ line ratio of $12 + \log(O/H) = 8.93 \pm 0.13$. The method used in our metallicity estimate is the same as the one used by MN11 to construct the FMR, in order to ensure a direct comparison. The estimated errors are purely based on the uncertainties of the mass and SFR, and any systematic uncertainties from the method used to fit the stellar mass have been ignored.

The agreement in the characteristic properties of the host galaxy of GRB 110918A with the FMR (see Fig. 6) shows that the host galaxy has no deficit of metals in comparison to normal field galaxies, in line with the conclusions of SG09, MN11, KR11, and Michałowski et al. (2012). This illustrates that the mass and SFR of a GRB-selected galaxy, at least for this one event, can be used as a fair proxy for the metallicity even in the solar, or super-solar regime.

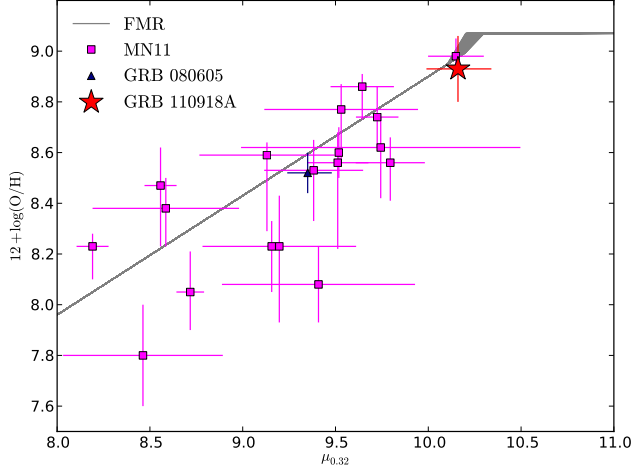


Fig. 6: The metallicity determined from the fundamental metallicity relation (taken from MN11) vs. the parametric quantity $\mu_{0.32}$, plotted in grey for a range of star formation rates (SFR = 0 – 100 $M_{\odot}\text{yr}^{-1}$). Real quantities are plotted for MN11 (magenta squares), GRB 080605 (Krühler et al. 2012a, cyan upward-pointing triangle), and GRB 110918A (red). The host of GRB 110918A is well described by the SDSS determined FMR.

4.4. Metallicity and Long GRB Progenitors

Many authors have attributed the fact that most long GRB host galaxies exhibit low metallicities as the result of an environmental preference, rather than the effect of the FMR (e.g., Modjaz et al. 2008; Graham & Fruchter 2012; Perley et al. 2013). This dependence on metallicity has also led to the prediction that the lower the progenitor metallicity, the larger the angular momentum, and thus the higher the energy output ($E_{\gamma,\text{iso}}$) of the GRB (MacFadyen & Woosley 1999). Initial studies indeed showed an anti-correlation between these two quantities (Stanek et al. 2006), together with a cut-off metallicity above which long GRBs (for $z < 0.2$) are no longer created, i.e., $Z < 0.15 Z_{\odot}$. More recent studies, however, which include long GRBs at cosmological redshifts and exclude sub-luminous GRBs (Wolf & Podsiadlowski 2007; Levesque et al. 2010c) indicate that there is no clear anti-correlation between metallicity and the GRB’s energy output, as shown in Fig. 7. The prompt emission of GRB 110918A yielded an energy output of $E_{\gamma,\text{iso}} = 1.9 \times 10^{54}$ erg (Frederiks & Pal’shin 2011) within the top 2% of the GRB population (Amati et al. 2008, Frederiks et al. 2013). This makes GRB 110918A one of the most energetic long GRBs yet observed and its host one of the most metal rich galaxies, in contradiction to the idea of a correlation between $E_{\gamma,\text{iso}}$ and metallicity.

Recently, Perley et al. (2013) performed an extensive photometric study of host galaxies selected from a sample of dark bursts, limiting the selection biases present in previous works. However, while the inclusion of dark GRB hosts increases the consistency of GRB hosts with the star formation weighted sample of field galaxies, there is still a clear lack of high-mass galaxies at $z \lesssim 1.5$. Associating the galaxy mass with metallicity, this provides indirect evidence for a metallicity effect in GRB hosts. A similar conclusion was reached based on a comparison of long GRB hosts with supernovae hosts (Graham & Fruchter 2012), namely that long GRB hosts show a strong preference for lower

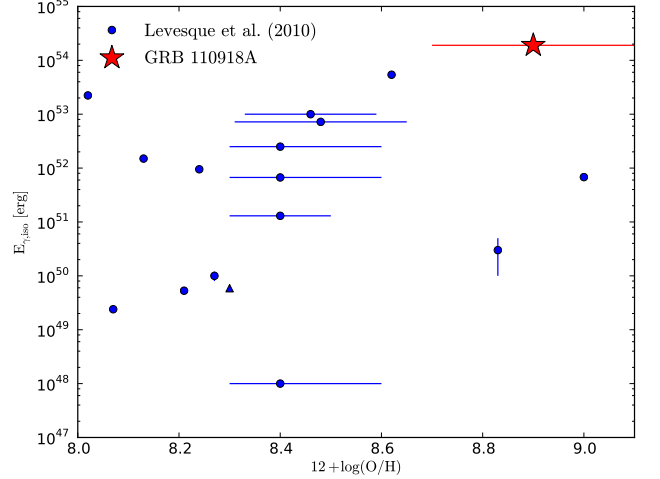


Fig. 7: The isotropic-equivalent energy release in γ -rays of GRBs plotted against the gas-phase metallicity of the host galaxy. Blue data are taken from Levesque et al. (2010c).

metallicity environments relative to other populations of star forming galaxies, with a metallicity cut-off of $Z < 0.5 Z_{\odot}$. This cut-off is not consistent with the host galaxy of GRB 110918A, even if metallicity dispersions of ~ 0.3 dex are considered (Niino 2011).

5. Conclusion

We observed the afterglow of GRB 110918A and its associated host galaxy and obtained photometry and spectroscopy of both. The extensive follow-up campaign has allowed us to measure the afterglow sight-line extinction as well as the attenuation of the galaxy’s stellar and gas-phase component. We further derive the host’s integrated SFR, stellar mass and gas-phase metallicity. In summary, this burst has revealed the following properties with respect to the long GRB population:

1. The SED determined stellar mass of $\log_{10}(M_{*}/M_{\odot}) = 10.68 \pm 0.16$ makes the host of GRB 110918A one of the most massive galaxies selected by a GRB at $z \sim 1$.
2. GRB 110918A is the first relatively unobscured afterglow ($A_V^{\text{GRB}} = 0.16$ mag) that has been detected in a very massive host galaxy, suggesting that the geometry of dust is more clumpy than homogeneous or local dust has been destroyed by the progenitor.
3. The optical/NIR spectrum reveals a solar metallicity environment ($0.9 - 1.7 Z_{\odot}$, depending on the chosen diagnostic), making it one of the most metal-rich long GRB host galaxies found yet.
4. Using the fundamental metallicity relation and the measured SFR, stellar mass and metallicity, we show that the host of GRB 110918A is no different to star forming galaxies selected through their own stellar light.
5. The large energy output from the γ -ray emission of GRB 110918A and the large metallicity content of the host galaxy, is in strong contradiction with there being an anti-correlation between energy output of the GRB and environmental metallicity.

6. Finally, the solar abundance of metals contradicts a cut-off for host galaxies of $Z < 0.5 Z_{\odot}$, even if a chemical dispersion of ~ 0.3 dex existed.

Acknowledgements. We thank the anonymous referees for their constructive criticisms, Régis Lachaume for the WFI observations, and Mara Salvato and Ivan Baldry for helpful discussions. Part of the funding for GROND (both hardware as well as personnel) was generously granted from the Leibniz-Prize to Prof. G. Hasinger (DFG grant HA 1850/28-1). Based on observations made with the Gran Telescopio Canarias (GTC), installed in the Spanish Observatorio del Roque de los Muchachos of the Instituto de Astrofísica de Canarias, in the island of La Palma. This work made use of data supplied by the UK Swift Science Data Centre at the University of Leicester. This publication makes use of data products from the Wide-field Infrared Survey Explorer, which is a joint project of the University of California, Los Angeles, and the Jet Propulsion Laboratory/California Institute of Technology, funded by the National Aeronautics and Space Administration. AdUP acknowledges support from a Marie Curie Career Integration Grant Fellowship. TK acknowledges support by the European Commission under the Marie Curie Intra-European Fellowship Programme. The Dark Cosmology Centre is funded by the Danish National Research Foundation. SS acknowledges support through project M.FE.A.Ext 00003 of the MPG. FOE acknowledges funding of his Ph.D. through the *Deutscher Akademischer Austausch-Dienst* (DAAD). AdUP, CT, RSR and JG acknowledge support from the Spanish research projects AYA2012-39362-C02-02, AYA2011-24780/ESP, AYA2009-14000-C03-01/ESP and AYA2010-21887-C04-01. AdUP acknowledges support from The Dark Cosmology Centre. KW acknowledges support by the STFC. PS acknowledges support by DFG grant SA 2001/1-1. DAK acknowledges support by the DFG cluster of excellence Origin and Structure of the Universe. SK, ANG, and AR acknowledge support by DFG grant Kl 766/16-1. AR, ANG, AK and DAK are grateful for travel funding support through MPE. MN acknowledges support by DFG grant SA 2001/2-1. EB acknowledges support from the National Science Foundation through Grant AST-1107973. JE is thankful for the support from A. and G. Elliott.

References

- Aihara, H., Allende Prieto, C., An, D., et al. 2011, *ApJS*, 193, 29
 Amati, L., Guidorzi, C., Frontera, F., et al. 2008, *MNRAS*, 391, 577
 Arnouts, S., Cristiani, S., Moscardini, L., et al. 1999, *MNRAS*, 310, 540
 Baade, D., Meisenheimer, K., Iwert, O., et al. 1999, *The Messenger*, 95, 15
 Barthelmy, S. D., Barbier, L. M., Cummings, J. R., et al. 2005, *Space Sci. Rev.*, 120, 143
 Basa, S., Cuby, J. G., Savaglio, S., et al. 2012, *A&A*, 542, A103
 Berger, E., Cowie, L. L., Kulkarni, S. R., et al. 2003, *ApJ*, 588, 99
 Bessell, M. S. 1979, *PASP*, 91, 589
 Bloom, J. S., Kulkarni, S. R., & Djorgovski, S. G. 2002, *AJ*, 123, 1111
 Bruzual, G. & Charlot, S. 2003, *MNRAS*, 344, 1000
 Burrows, D. N., Hill, J. E., Nousek, J. A., et al. 2005, *Space Sci. Rev.*, 120, 165
 Butler, N. R., Bloom, J. S., & Poznanski, D. 2010, *ApJ*, 711, 495
 Calzetti, D., Armus, L., Bohlin, R. C., et al. 2000, *ApJ*, 533, 682
 Cepa, J., Aguiar, M., Escalera, V. G., et al. 2000, in *Society of Photo-Optical Instrumentation Engineers (SPIE) Conference Series*, Vol. 4008, Society of Photo-Optical Instrumentation Engineers (SPIE) Conference Series, ed. M. Iye & A. F. Moorwood, 623–631
 Chabrier, G. 2003, *PASP*, 115, 763
 Christensen, L., Fynbo, J. P. U., Prochaska, J. X., et al. 2011, *ApJ*, 727, 73
 Christensen, L., Hjorth, J., & Gorosabel, J. 2004, *A&A*, 425, 913
 Cucchiara, A., Prochaska, J. X., Zhu, G., et al. 2012, *MNRAS*, 426, 2078
 Daigne, F., Rossi, E. M., & Mochkovitch, R. 2006, *MNRAS*, 372, 1034
 de Ugarte Postigo, A., Fynbo, J. P. U., Thöne, C. C., et al. 2012, *A&A*, 548, A11
 Della Valle, M. 2011, *International Journal of Modern Physics D*, 20, 1745
 Elliott, J., Greiner, J., Khochfar, S., et al. 2012, *A&A*, 539, A113
 Elliott, J., Kruehler, T., Klose, S., et al. 2011, *GRB Coordinates Network*, 12366, 1
 Erb, D. K., Shapley, A. E., Pettini, M., et al. 2006, *ApJ*, 644, 813
 Filgas, R., Greiner, J., Schady, P., et al. 2011, *A&A*, 535, A57
 Filippenko, A. V. 1997, *ARA&A*, 35, 309
 Frederiks, D. & Pal'shin, V. 2011, *GRB Coordinates Network*, 12370, 1
 Fruchter, A. S., Thorsett, S. E., Metzger, M. R., et al. 1999, *ApJ*, 519, L13
 Fynbo, J. P. U., Jakobsson, P., Prochaska, J. X., et al. 2009, *ApJS*, 185, 526
 Galama, T. J., Vreeswijk, P. M., van Paradijs, J., et al. 1998, *Nature*, 395, 670
 Garn, T. & Best, P. N. 2010, *MNRAS*, 409, 421
 Gehrels, N., Chincarini, G., Giommi, P., et al. 2004, *ApJ*, 611, 1005
 Goldoni, P., Royer, F., François, P., et al. 2006, in *SPIE Conf. Ser.*, Vol. 6269
 Golenetskii, S., Aptekar, R., Frederiks, D., et al. 2011, *GRB Coordinates Network*, 12362, 1
 Graham, J. F. & Fruchter, A. S. 2012, *ApJ*, submitted (arXiv:1211.7086)
 Greiner, J., Bornemann, W., Clemens, C., et al. 2008, *PASP*, 120, 405
 Greiner, J., Krühler, T., Klose, S., et al. 2011, *A&A*, 526, A30
 Hirschi, R., Meynet, G., & Maeder, A. 2005, *A&A*, 443, 581
 Hjorth, J., Malesani, D., Jakobsson, P., et al. 2012, *ApJ*, 756, 187
 Hjorth, J., Sollerman, J., Møller, P., et al. 2003, *Nature*, 423, 847
 Hogg, D. W., Pahre, M. A., McCarthy, J. K., et al. 1997, *MNRAS*, 288, 404
 Hook, I. M., Jørgensen, I., Allington-Smith, J. R., et al. 2004, *PASP*, 116, 425
 Hurley, K., Golenetskii, S., Aptekar, R., et al. 2011, *GRB Coordinates Network*, 12357, 1
 Ilbert, O., Arnouts, S., McCracken, H. J., et al. 2006, *A&A*, 457, 841
 Ilbert, O., Capak, P., Salvato, M., et al. 2009, *ApJ*, 690, 1236
 Ishida, E. E. O., de Souza, R. S., & Ferrara, A. 2011, *MNRAS*, 418, 500
 Jarrett, T. H., Masci, F., Tsai, C. W., et al. 2012, *AJ*, 144, 68
 Kalberla, P. M. W., Burton, W. B., Hartmann, D., et al. 2005, *A&A*, 440, 775
 Kann, D. A., Klose, S., & Zeh, A. 2006, *ApJ*, 641, 993
 Kann, D. A., Klose, S., Zhang, B., et al. 2010, *ApJ*, 720, 1513
 Kennicutt, Jr., R. C. 1998, *ARA&A*, 36, 189
 Kewley, L. J. & Dopita, M. A. 2002, *ApJS*, 142, 35
 Kewley, L. J. & Ellison, S. L. 2008, *ApJ*, 681, 1183
 Kistler, M. D., Yüksel, H., Beacom, J. F., Hopkins, A. M., & Wytthe, J. S. B. 2009, *ApJ*, 705, L104
 Kocevski, D. & West, A. A. 2011, *ApJ*, 735, L8+
 Krimm, H. A. & Siegel, H. v. M. 2011, *GCN Report*, 350, 1
 Krühler, T., Fynbo, J. P. U., Geier, S., et al. 2012a, *A&A*, 546, A8
 Krühler, T., Greiner, J., Schady, P., et al. 2011, *A&A*, 534, A108
 Krühler, T., Küpcü Yoldaş, A., Greiner, J., et al. 2008, *ApJ*, 685, 376
 Krühler, T., Malesani, D., Milvang-Jensen, B., et al. 2012b, *ApJ*, 758, 46
 Le Floc'h, E., Duc, P.-A., Mirabel, I. F., et al. 2003, *A&A*, 400, 499
 Levesque, E. M., Berger, E., Kewley, L. J., & Bagley, M. M. 2010a, *AJ*, 139, 694
 Levesque, E. M., Kewley, L. J., Berger, E., & Zahid, H. J. 2010b, *AJ*, 140, 1557
 Levesque, E. M., Soderberg, A. M., Kewley, L. J., & Berger, E. 2010c, *ApJ*, 725, 1337
 Li, L. 2008, *MNRAS*, 388, 1487
 MacFadyen, A. I. & Woosley, S. E. 1999, *ApJ*, 524, 262
 Mangano, V., Sbarufatti, B., Evans, P. A., & Krimm, H. A. 2011, *GRB Coordinates Network*, 12364, 1
 Mannucci, F., Salvaterra, R., & Campisi, M. A. 2011, *MNRAS*, 439
 Matheson, T., Garnavich, P. M., Stanek, K. Z., et al. 2003, *ApJ*, 599, 394
 Michałowski, M. J., Kamble, A., Hjorth, J., et al. 2012, *ApJ*, 755, 85
 Modjaz, M., Kewley, L., Kirshner, R. P., et al. 2008, *AJ*, 135, 1136
 Nagao, T., Maiolino, R., & Marconi, A. 2006, *A&A*, 459, 85
 Nestor, D. B., Johnson, B. D., Wild, V., et al. 2011, *MNRAS*, 412, 1559
 Niino, Y. 2011, *MNRAS*, 417, 567
 Oksanen, A., Schaefer, B., Harlinton, C., & Templeton, M. 2011, *GRB Coordinates Network*, 12458, 1
 Osterbrock, D. E. 1989, *Astrophysics of gaseous nebulae and active galactic nuclei*
 Paczynski, B. 1998, *ApJ*, 494, L45+
 Pei, Y. C. 1992, *ApJ*, 395, 130
 Perley, D. A., Cenko, S. B., Bloom, J. S., et al. 2009, *AJ*, 138, 1690
 Perley, D. A., Levan, A. J., Tanvir, N. R., et al. 2013, *ApJ*, submitted (arXiv:1301.5903)
 Pettini, M. & Pagel, B. E. J. 2004, *MNRAS*, 348, L59
 Robertson, B. E. & Ellis, R. S. 2012, *ApJ*, 744, 95
 Rodríguez Hidalgo, P., Wessels, K., Charlton, J. C., et al. 2012, *MNRAS*, 427, 1801
 Rossi, A., Klose, S., Ferrero, P., et al. 2012, *A&A*, 545, A77
 Salvaterra, R., Campana, S., Vergani, S. D., et al. 2012, *ApJ*, 749, 68
 Savaglio, S., Glazebrook, K., & Le Borgne, D. 2009, *ApJ*, 691, 182
 Savaglio, S., Glazebrook, K., Le Borgne, D., et al. 2005, *ApJ*, 635, 260
 Schady, P., Dwelly, T., Page, M. J., et al. 2012, *A&A*, 537, A15
 Schlegel, D. J., Finkbeiner, D. P., & Davis, M. 1998, *ApJ*, 500, 525
 Skrutskie, M. F., Cutri, R. M., Stiening, R., et al. 2006, *AJ*, 131, 1163
 Stanek, K. Z., Gnedin, O. Y., Beacom, J. F., et al. 2006, *Acta Astron.*, 56, 333
 Stanek, K. Z., Matheson, T., Garnavich, P. M., et al. 2003, *ApJ*, 591, L17
 Sudilovsky, V., Greiner, J., Rau, A., et al. 2013, *A&A*, 552, A143
 Tanvir, N. R., Barnard, V. E., Blain, A. W., et al. 2004, *MNRAS*, 352, 1073
 Tanvir, N. R., Levan, A. J., Fruchter, A. S., et al. 2012, *ApJ*, 754, 46
 Tanvir, N. R., Wiersema, K., Levan, A. J., Greiss, S., & Gaensicke, B. 2011, *GRB Coordinates Network*, 12365, 1
 Tody, D. 1993, in *Astronomical Society of the Pacific Conference Series*, Vol. 52, *Astronomical Data Analysis Software and Systems II*, ed. R. J. Hanisch, R. J. V. Brissenden, & J. Barnes, 173
 Tremonti, C. A., Heckman, T. M., Kauffmann, G., et al. 2004, *ApJ*, 613, 898

Vernet, J., Dekker, H., D’Odorico, S., et al. 2011, *A&A*, 536, A105
 Wang, F. Y. & Dai, Z. G. 2011, *ApJ*, 727, L34+
 Wigger, C., Wigger, O., Bellm, E., & Hajdas, W. 2008, *ApJ*, 675, 553
 Wolf, C. & Podsiadlowski, P. 2007, *MNRAS*, 375, 1049
 Woosley, S. E. 1993, *ApJ*, 405, 273
 Woosley, S. E. & Heger, A. 2006, *ApJ*, 637, 914
 Wright, E. L., Eisenhardt, P. R. M., Mainzer, A. K., et al. 2010, *AJ*, 140, 1868
 Yabe, K., Ohta, K., Iwamuro, F., et al. 2012, *PASJ*, 64, 60
 Yoldaş, A. K., Krühler, T., Greiner, J., et al. 2008, in *American Institute of Physics Conference Series*, Vol. 1000, American Institute of Physics Conference Series, ed. M. Galassi, D. Palmer, & E. Fenimore, 227–231
 Yoon, S.-C. & Langer, N. 2005, *A&A*, 443, 643
 Zahid, H. J., Yates, R. M., Kewley, L. J., & Kudritzki, R. P. 2013, *ApJ*, 763, 92

Appendix C: The Host’s Emission Lines

Two spectra of the host galaxy were obtained with OSIRIS and X-shooter (see Sect. 3.3), showing the following emission lines: $H\alpha$ and $H\beta$ transitions from the Balmer series and also forbidden transitions of [O II] and [N II] (only [O II] emission was detected with OSIRIS, and so for consistency only the X-shooter emission lines are shown). All of the 2D spectral images and 1D Gaussian fits can be seen in Fig C.1.

Appendix A: The Afterglow Light Curve

The afterglow of GRB 110918A was imaged for over 40 days after the trigger with GROND in the $g'r'i'z'JHK_s$ bands (outlined in Sect. 2.2). Utilising the deep observations of the host, the underlying contribution from the host galaxy was subtracted using the High Order Transform of PSF and Template Subtraction package, HOTPANTS¹¹ v5.1.10b. The resulting afterglow light curve can be seen in Fig. A.1, the raw data can be found in Tables A.2 and A.3 and the host subtracted data can be found in Tables A.4 and A.5. The standard stars used in $g'r'i'z'$ for relative calibration can be found in Table A.1.

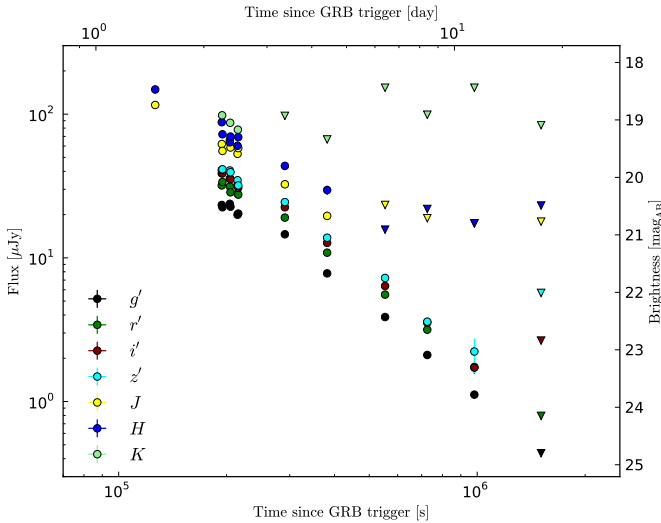


Fig. A.1: The afterglow light curve of GRB 110918A obtained with the 7 channel imager GROND (host subtracted).

Appendix B: The Afterglow’s Sight-Line Spectrum

The spectra obtained with GMOS and OSIRIS (see Sect. 2.6) reveal many absorption lines of gas along the line of sight toward the afterglow, specifically of the following species: Fe II (2344,2374,2382,2586,2600), Mg II (2803,2796), Mg I (2853) and Ca II (3935,3970). The equivalent widths of the metals are listed in Table B.1.

¹¹ <http://www.astro.washington.edu/users/becker/hotpants.html>

Table A.1: Optical reference stars.

R.A. (J2000)	Dec. (J2000)	g' mag _{AB}	r' mag _{AB}	i' mag _{AB}	z' mag _{AB}
02:10:16.65	-27:06:22.7	19.85 ± 0.03	19.64 ± 0.03	19.53 ± 0.04	19.54 ± 0.04
02:10:11.56	-27:04:53.9	20.28 ± 0.03	19.86 ± 0.03	19.72 ± 0.04	19.72 ± 0.05
02:10:13.25	-27:07:04.0	19.82 ± 0.03	19.48 ± 0.03	19.30 ± 0.03	19.27 ± 0.04
02:10:12.62	-27:08:12.2	20.83 ± 0.04	19.37 ± 0.03	17.96 ± 0.03	17.27 ± 0.03

Table A.2: GROND photometric data $g'r'i'z'$.

$T_{mid} - T_0$ s	Exposure s	g' mag _{AB}	r' mag _{AB}	i' mag _{AB}	z' mag _{AB}
193892	691	20.43 ± 0.04	20.15 ± 0.02	19.92 ± 0.04	19.80 ± 0.07
194311	1526	20.39 ± 0.04	20.16 ± 0.03	19.93 ± 0.03	19.73 ± 0.08
194724	699	20.42 ± 0.03	20.18 ± 0.02	19.92 ± 0.04	19.80 ± 0.06
204203	683	20.48 ± 0.03	20.25 ± 0.02	20.05 ± 0.03	19.87 ± 0.06
204615	1508	20.48 ± 0.03	20.25 ± 0.02	20.02 ± 0.03	19.84 ± 0.06
205025	689	20.51 ± 0.03	20.28 ± 0.02	20.02 ± 0.03	19.89 ± 0.06
214526	693	20.56 ± 0.03	20.33 ± 0.02	20.09 ± 0.04	19.98 ± 0.06
215017	1674	20.56 ± 0.04	20.33 ± 0.02	20.11 ± 0.03	19.90 ± 0.07
215504	700	20.56 ± 0.05	20.32 ± 0.03	20.12 ± 0.04	19.91 ± 0.07
290361	691	21.09 ± 0.02	20.81 ± 0.02	20.66 ± 0.03	20.40 ± 0.06
290775	1519	21.11 ± 0.03	20.88 ± 0.03	20.65 ± 0.04	20.44 ± 0.06
291188	693	21.09 ± 0.03	20.83 ± 0.02	20.62 ± 0.03	20.44 ± 0.05
381456	1727	21.60 ± 0.02	21.30 ± 0.02	21.06 ± 0.03	20.96 ± 0.05
553350	1732	22.19 ± 0.04	21.96 ± 0.03	21.59 ± 0.06	21.30 ± 0.07
725709	1727	22.62 ± 0.05	22.46 ± 0.05	22.02 ± 0.09	21.54 ± 0.10
981853	3455	22.89 ± 0.06	22.76 ± 0.07	22.02 ± 0.09	21.60 ± 0.09
1507300	5327	23.09 ± 0.07	22.84 ± 0.08	22.05 ± 0.07	21.75 ± 0.09

Notes. All magnitudes have been corrected for Galactic foreground reddening. No correction has been made to subtract the flux contribution from the underlying host galaxy.

Table A.3: GROND photometric data JHK_s .

$T_{mid} - T_0$ s	Exposure s	J mag _{AB}	H mag _{AB}	K_s mag _{AB}
126393	82	18.93 ± 0.08	18.76 ± 0.08
194337	1579	19.40 ± 0.09	19.18 ± 0.12	18.84 ± 0.15
204643	1560	19.50 ± 0.08	19.19 ± 0.12	18.90 ± 0.16
215045	1726	19.58 ± 0.10	19.35 ± 0.12	18.84 ± 0.15
290803	1571	19.78 ± 0.09	19.64 ± 0.12	18.90 ± 0.16
381482	1773	20.21 ± 0.10	19.73 ± 0.16	19.03 ± 0.16
553375	1779	20.53 ± 0.14	20.17 ± 0.17	19.25 ± 0.19
725734	1774	20.82 ± 0.16	20.43 ± 0.21	19.64 ± 0.19
981879	3455	21.08 ± 0.15	20.59 ± 0.18	19.56 ± 0.28
1507330	5379	20.77 ± 0.12	20.65 ± 0.16	19.50 ± 0.27

Notes. All magnitudes have been corrected for Galactic foreground reddening. No correction has been made to subtract the flux contribution from the underlying host galaxy.

Table A.4: GROND host subtracted photometric data $g'r'i'z'$.

$T_{mid} - T_0$	Exposure	g'	r'	i'	z'
193892	691	20.48 ± 0.04	20.14 ± 0.02	19.93 ± 0.02	19.87 ± 0.03
194724	699	20.52 ± 0.03	20.08 ± 0.03	19.93 ± 0.03	19.86 ± 0.04
204203	683	20.46 ± 0.04	20.16 ± 0.02	20.02 ± 0.02	19.88 ± 0.05
205025	689	20.51 ± 0.04	20.26 ± 0.02	20.03 ± 0.03	19.91 ± 0.04
214527	693	20.65 ± 0.03	20.28 ± 0.02	20.13 ± 0.03	20.05 ± 0.03
215504	700	20.63 ± 0.04	20.30 ± 0.02	20.18 ± 0.03	20.14 ± 0.04
290776	1519	20.99 ± 0.04	20.70 ± 0.03	20.52 ± 0.03	20.43 ± 0.04
381457	1727	21.67 ± 0.03	21.31 ± 0.02	21.14 ± 0.03	21.05 ± 0.04
553350	1732	22.43 ± 0.04	22.04 ± 0.03	21.89 ± 0.04	21.75 ± 0.05
725709	1727	23.09 ± 0.05	22.65 ± 0.04	22.53 ± 0.06	22.51 ± 0.06
981853	3455	23.78 ± 0.06	23.30 ± 0.06	23.31 ± 0.10	23.03 ± 0.28
1507300	5327	> 24.80	> 24.15	> 22.84	> 22.01

Notes. All magnitudes have been corrected for Galactic foreground reddening.

Table A.5: GROND host subtracted photometric data JHK_s .

$T_{mid} - T_0$	Exposure	J	H	K_s
s	s	mag _{AB}	mag _{AB}	mag _{AB}
126444	393	18.74 ± 0.05	18.47 ± 0.07
193921	745	19.42 ± 0.06	19.04 ± 0.05
194338	790	18.92 ± 0.08
194751	752	19.54 ± 0.06	19.25 ± 0.06
204231	736	19.35 ± 0.06	19.39 ± 0.06
204643	780	19.05 ± 0.07
205052	742	19.48 ± 0.06	19.29 ± 0.06
214555	746	19.59 ± 0.06	19.45 ± 0.08
215045	863	19.17 ± 0.07
215531	753	19.49 ± 0.06	19.30 ± 0.06
290803	1571	20.12 ± 0.08	19.80 ± 0.07	> 18.93
381482	1773	20.67 ± 0.10	20.22 ± 0.08	> 19.34
553375	1779	> 20.48	> 20.91	> 18.44
725734	1774	> 20.71	> 20.55	> 18.91
981879	3455	> 20.80	> 20.80	> 18.44
1507329	5379	> 20.77	> 20.49	> 19.09

Notes. All magnitudes have been corrected for Galactic foreground reddening.

Table B.1: Equivalent widths measured for the absorption lines of the afterglow.

λ_{obs}	Feature	Contaminants	EW _{obs}	EW _{rest}	z
Å					
4650.4	Fe II2344.2	Fe II*2345.0	4.3 ± 0.4	2.2 ± 0.2	0.9838
4713.4	Fe II2374.5 [†]	0.9850
4720.5	Fe II*2381.5	8.4 ± 0.6	4.2 ± 0.3
4727.2	Fe II2382.8 [†]	0.9389
5132.7	Fe II2586.7	Mn II2594.5	3.7 ± 0.4	1.9 ± 0.2	0.9843
5157.7	Fe II2600.2	Mn II2696.7, Fe II*2586.7	6.3 ± 0.5	3.2 ± 0.2	0.9836
5547.3	Mg II2796.4 [†]	0.9837
5540.8	11.9 ± 0.4	6.0 ± 0.2
5560.1	Mg II2803.5 [†]	0.9833
5660.2	Mg I2853.0	4.3 ± 0.4	2.2 ± 0.2	0.9840
7806.1	Ca II3934.8	4.0 ± 0.5	2.0 ± 0.2	0.9839
7877.6	Ca II3969.6	3.3 ± 0.6	1.7 ± 0.3	0.9845

Notes. The redshift was determined for those lines with no contaminants. ^(†) Blended lines.

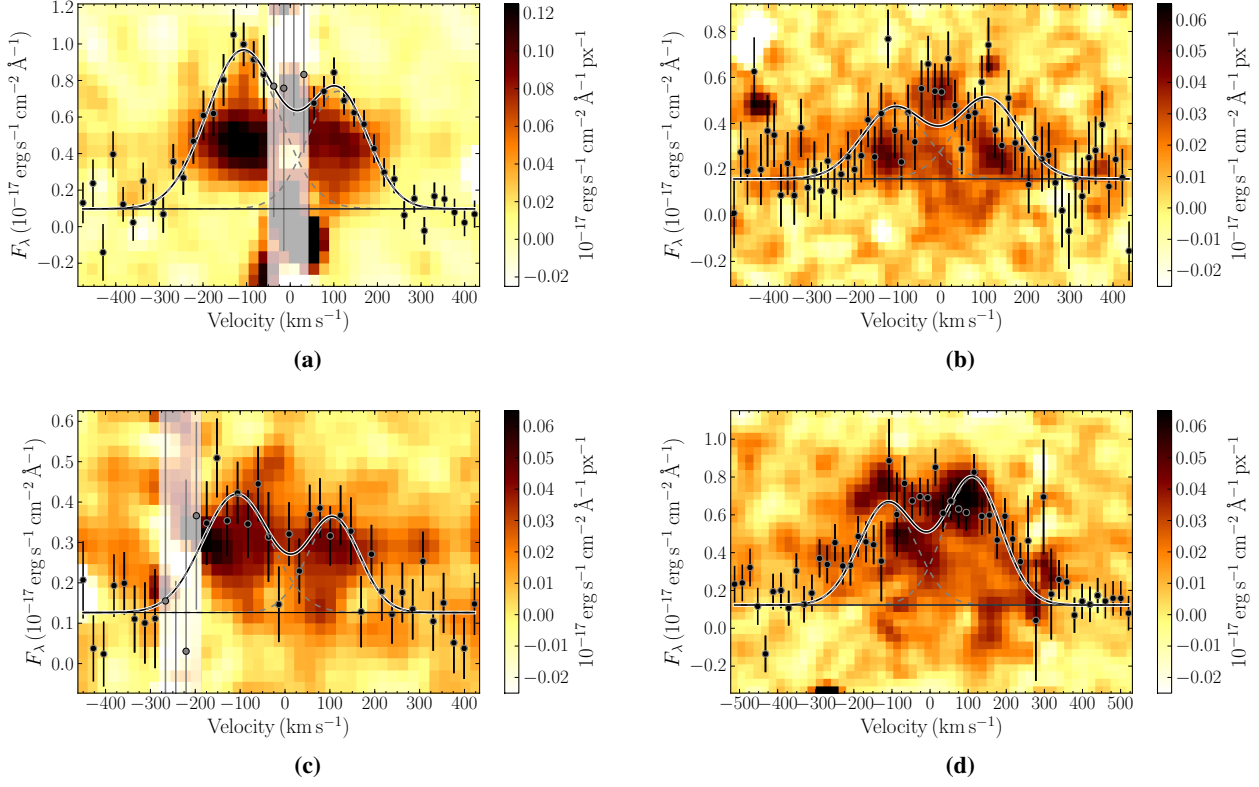


Fig. C.1: The 2D spectra of the host of GRB 110918A, depicting four different emissions ([N II], [O II], H α , H β). Overplotted is our Gaussian fit where areas that overlay telluric lines are shown in white and excluded from the fit. All the values presented are raw values and do not include slit-loss or extinction corrections. Each image has been smoothed in both pixel directions for presentation purposes. **(a):** The Balmer series transition H α . **(b):** The Balmer series transition H β . **(c):** The forbidden transition [N II]. **(d):** The forbidden transition [O II].